THE INTERNAL VELOCITY DISPERSIONS OF THREE YOUNG STAR CLUSTERS IN THE LARGE MAGELLANIC CLOUD

ROBERT H. LUPTON
Institute for Astronomy, University of Hawaii

S. MICHAEL FALL
Space Telescope Science Institute

KENNETH C. FREEMAN
Mount Stromlo and Siding Spring Observatories, and Space Telescope Science Institute

AND

REBECCA A. W. ELSON
Institute for Advanced Study
Received 1989 February 21; accepted 1989 June 2

ABSTRACT

We have measured the radial velocities of 11 to 37 stars in each of three rich young star clusters in the Large Magellanic Cloud (LMC): NGC 1866, NGC 2164, and NGC 2214. The observational errors (a few km s^{-1}) are comparable to the observed velocity dispersions and the samples are probably contaminated by a few field stars. Under these circumstances, we can only set upper limits on the true velocity dispersions within the clusters. The methods presented here should be useful in a variety of contexts where velocity dispersions are difficult to measure. Our limits for all three LMC clusters are $\sigma_v \lesssim 3$ to 4 km s^{-1} at the 95% confidence level. Combining these results with the surface brightness profiles derived in an earlier study, we find upper limits on the total masses of 6×10^5, 2×10^5, and 4×10^5 $M_\odot$, respectively, for NGC 1866, NGC 2164, and NGC 2214. The corresponding limits on the global mass-to-light ratios are 0.5, 0.7, and 1.3 in solar units. From the small velocity dispersion and large radial extent of NGC 1866, we infer that the cluster is not yet tidally limited by the LMC. This confirms a previous suggestion by Elson, Fall, and Freeman, which was based on mass-to-light ratios derived from stellar population models. The other clusters in our sample, NGC 2164 and NGC 2214, may also have unbound halos, but our limits on the velocity dispersions are not tight enough to draw definite conclusions.

Subject headings: clusters: dynamics — clusters: open — galaxies: Magellanic Clouds

I. INTRODUCTION

The velocity dispersion and surface brightness profile of a star cluster can be combined to obtain a direct indication of its mass. Other methods, involving tidal radii or stellar population models, provide less reliable estimates. The velocity dispersions of many Galactic globular clusters have now been measured, either from the broadening of absorption lines in the integrated spectra (Illingworth 1976) or from the radial velocities of individual stars (Lupton, Gunn, and Griffin 1987, and references therein). A velocity dispersion has been derived from the integrated spectrum of the old LMC cluster NGC 1835 (Elson and Freeman 1985). Since the young clusters in the LMC provide valuable clues about the formation and early evolution of globular-like clusters, it is important to determine as many of their properties as possible, including their masses and mass-to-light ratios. However, the light of clusters younger than 10^9 yr is dominated by A to early-F stars, which have weak metal lines, and the velocity dispersions cannot be derived from the integrated spectra. In this paper, we present measurements of the radial velocities of 11 to 37 stars in each of the clusters NGC 1866, NGC 2164, and NGC 2214. They have ages of a few times 10^7 yr, are typical of the richest clusters in the LMC, and lie in relatively uncrowded fields.

One motivation for determining the velocity dispersions of young LMC clusters comes from the recent study by Elson, Fall, and Freeman (1987, hereafter EFF). They analyzed aperture photometry and star counts for 10 clusters and found that King models gave poor fits to most of the surface brightness profiles at large radii. Instead, the observed profiles could be represented by the simple formula

$$\mu(R) = \mu_0[1 + (R/a)^2]^{-\gamma/2} . \tag{1}$$

Table 1 lists for the three clusters in our sample the central surface brightness μ_0, the power-law index γ, and the parameter a, which is related to the core radius by $r_c = a(2^{2/\gamma} - 1)^{1/2}$. Also listed are the age τ, the radius containing half the light in three dimensions r_h, the radius to which the cluster could be distinguished from the background r_{max}, and the "asymptotic" (integrated) luminosity $L_{V\infty}$, obtained by extrapolating the profiles beyond r_{max}. One reason for selecting the three clusters in our sample is that their structural parameters are reasonably well determined. With the possible exception of NGC 1866, there is no evidence for mass segregation within the clusters.

The limiting radius of a star cluster depends on its mean density, its orbit, and the tidal field of the parent galaxy. Even if the gas cloud from which the cluster formed was tidally limited, any subsequent mass loss, driven for example by stellar winds or

201

TABLE 1

OBSERVED PROPERTIES OF THE CLUSTERS

Quantity	NGC 1866	NGC 2164	NGC 2214
γ	2.55	2.80	2.40
$\log(\mu_0/L_\odot \, \mathrm{pc}^{-2})$	3.64	3.87	3.42
a/arcsec	17	9	11
r_h/arcsec	63	22	100:
r_{max}/arcsec	500	250	350
$\log(L_{V\infty}/L_\odot)$	6.0	5.5	5.6
$\log(\tau/\mathrm{yr})$	7.7	7.5	7.5

NOTE.—All entries are from Elson, Fall, and Freeman 1987, 1989.

supernovae, would cause the cluster to expand and spill over its Roche surface. The unbound halo thus formed would probably survive for several orbits of the cluster around the parent galaxy. As a test of this possibility, EFF used the mass-to-light ratios from stellar population models to estimate the densities of the young LMC clusters. They found that, for wide ranges of slopes and upper and lower cutoffs of the initial mass functions (IMFs), most of the clusters extend beyond their eventual tidal radii. This is consistent with the absence of truncation at large radii in most of the observed profiles and the good fits provided by equation (1). However, the mass-to-light ratios used by EFF were uncertain by more than an order of magnitude and the inferred tidal radii by factors of about 3. Even with the IMF slopes recently estimated by Elson, Fall, and Freeman (1989), the uncertainties are still significant because the upper and lower mass cutoffs are not known. One of the main goals of this paper is to use the internal velocity dispersions of the young LMC clusters to place stronger constraints on their eventual tidal radii.

In § II, we describe our observations and the methods used to derive radial velocities from them. Accurate measurements are required because the expected velocity dispersions within the clusters are only a few km s^{-1}. In § III, we present a thorough analysis of the observational errors and contamination by field stars and a new method to assign confidence limits to the velocity dispersions. In § IV, we set limits on the central densities, total masses, and mass-to-light ratios of the clusters, and in § V, we focus on the question of whether they have unbound halos. Throughout this paper we adopt for the LMC a distance modulus of 18.7, which corresponds to a distance of 55 kpc. Since values as small as $m - M = 18.2$ are possible, we often note the dependence of our results on the distance to the LMC. Our main conclusions are not affected by this uncertainty.

II. OBSERVATIONS AND DATA REDUCTION

Color-magnitude diagrams from Robertson (1974) and Flower and Hodge (1975) were used to identify the G and K supergiants in the three clusters in our sample. These are the most suitable stars for determining radial velocities because they are relatively bright and have narrow absorption lines. We have observed, respectively, 37, 16, and 11 stars in NGC 1866, NGC 2164, and NGC 2214. The x and y coordinates with respect to the centers of the clusters and the V magnitudes and $B-V$ colors of the program stars are listed in Tables 2a–2c. Their positions are shown in Figures 1a–1c, where we have also plotted circles of radii r_h. Most of the program stars lie within $2r_h$ of the centers of the clusters, but only a few of them lie within the cores. As a result, the velocity dispersions discussed below are " global " rather than " central."

Spectra of the program stars in NGC 1866 and NGC 2164 were obtained on 1986 December 4 and 5 using the RGO spectrograph, the multiple-fiber system, and the Image Photon Counting System (IPCS) at the Cassegrain focus of the 3.9 m Anglo-Australian Telescope. The 25 cm camera, with the 1200 V grating in first order, gave a dispersion of 0.5 Å per (15 μm) channel and a total wavelength coverage of 4950–5600 Å. The fibers were 400 μm or 2".7 in diameter, and the FWHM of the instrumental profile was about 1.5 Å. Integrations on the program stars, separated by exposures of Cu-Ar-Ne lamps, were 1500 s. Three fibers placed in dark areas near the clusters provided the mean sky spectrum. Integrations on the twilight sky were used to measure the relative transmission of all the fibers. For NGC 2214, the observations were made on 1988 January 18, with a similar setup, but without fibers, because the program stars were too close together. Typical integration times for this cluster were 1000 s.

We obtained two independent sets of data for both NGC 1866 and NGC 2164 with different placements of the fibers in the aperture plates. We refer to these as " permutations " of the fibers. The resulting spectra, reduced separately as described below, play a crucial role in the error analysis of the next section. We made four integrations of all the program stars in NGC 1866 with one permutation and four with another. For NGC 2164, the minimum separation between the fibers, about 19", did not allow us to observe all the stars at once. Three integrations were made on December 4 with one permutation of fibers, and another three integrations were made on December 5 with a second permutation. These had only seven stars in common, and unfortunately, there was not enough time to obtain a second set of observations of the remaining program stars. We have two independent observations of six stars in NGC 2214.

The observations were reduced using a combination of the FIGARO, PANDORA, and STARLINK software packages. For NGC 1866 and NGC 2164, we first used the quartz-lamp flat field exposures to determine the positions of the individual fiber spectra and to extract them from the IPCS frames. The means of the arc spectra taken before and after each integration were used to place the sky and stellar spectra on a logarithmic wavelength scale. We then subtracted the mean sky spectra, scaled by the transmission of each fiber, from the stellar spectra. The sky contributed less than 20% of the total signal, and the bright sky line at 5577 Å provided a check on the subtraction. We added the spectra of each star, separately for each permutation of the fibers, and then determined the velocities relative to a template spectrum for each cluster using a Fourier transform/cross-correlation routine. The templates were constructed by shifting and adding the spectra of all the program stars in NGC 1866 and NGC 2164. For
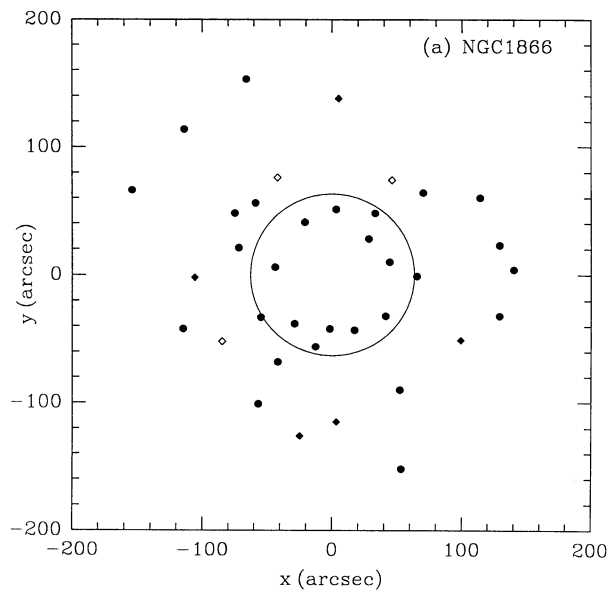
FIG. 1a
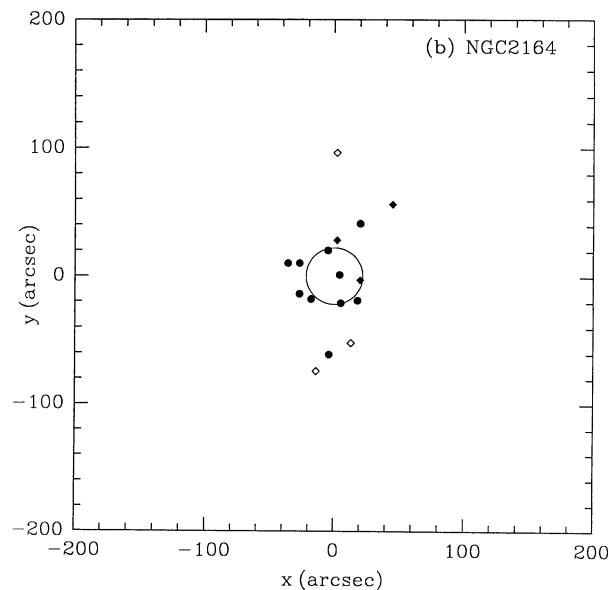
FIG. 1b
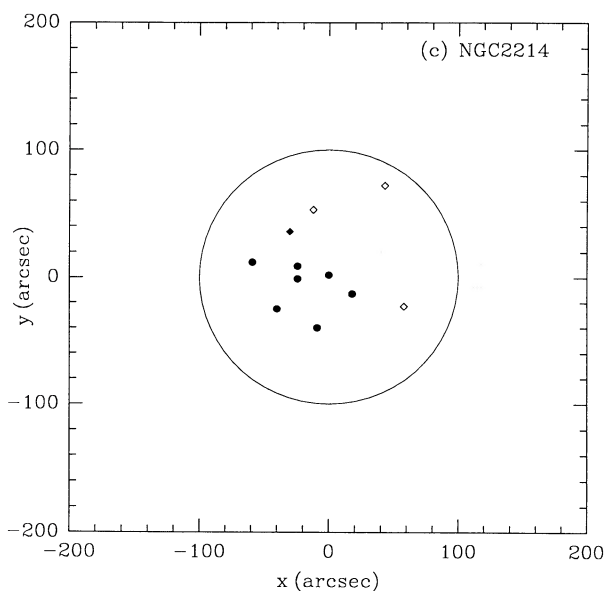
FIG. 1c

FIG. 1.—(a–c) Positions of the program stars relative to the centers of the clusters for (a) NGC 1866, (b) NGC 2164, and (c) NGC 2214. The coordinates x and y increase to the east and north respectively. Probable cluster members are indicated by filled circles, probable LMC field stars by filled diamonds, and Galactic field stars by open diamonds. The circles have radii equal to r_h.

NGC 2214, the velocities were determined in much the same way except that the template consisted of the summed spectra of three giants in the Galactic cluster M67, observed on the same night as the program stars. This avoids any problems that might be caused by autocorrelations in a small sample.

The adopted velocities of the program stars are listed in Tables 2a–2c. These are the means $v = \frac{1}{2}(v_I + v_{II})$ of our two independent measurements, when available, and otherwise, they are the results of single observations. The velocities of the program stars in each cluster have a common zeropoint that was chosen, somewhat arbitrarily, to be near the mean velocity of the cluster. Also listed in Tables 2a–2c are the differences $\delta = \frac{1}{2}(v_I - v_{II})$, which we use in the next section to estimate the errors in the velocities. We omit star CII-20 in NGC 1866 from further consideration because at least one of the measurements is clearly in error.

<center>III. ERROR ANALYSIS AND VELOCITY DISPERSIONS</center>

<center>a) Measurement Errors</center>

We must consider the measurement errors in some detail because the expected velocity dispersions within the clusters are only a few km s^{-1}. Errors in the velocities of individual stars are caused by photon noise, effects inherent in the fiber/spectrograph system, and uncertainties in the wavelength calibration. The latter were estimated by cross-correlating the arc spectra in the same manner as the stellar spectra. For the fiber spectra, the standard deviation of the wavelength differences was 1.1 km s^{-1}, and for the slit spectra,

TABLE 2

A. PROGRAM STARS FOR NGC 1866

Star (1)	x (arcsec) (2)	y (arcsec) (3)	V (4)	B−V (5)	v (km s⁻¹) (6)	δ (km s⁻¹) (7)
BI-28	+41	−32	16.60	1.03	+0.7	+2.5
BI-36	+17	−43	15.72	1.37	+3.6	+3.3
BII-8	−13	−56	16.56	1.09	+6.3	−4.3
BII-12	−2	−42	16.27	0.99	+9.8	−0.6
BII-20	−42	−68	16.32	1.18	+2.2	−0.4
BII-40	−55	−33	15.55	1.14	+0.4	+2.2
BII-64	−29	−38	15.82	0.82	+5.5	−2.0
BIII-2	−75	+48	16.69	1.00	+2.6	+0.6
BIII-5	−59	+56	15.92	1.16	+5.9	−5.9
(BIII-7)	−42	+76	16.99	1.26	−250.4	+3.3
BIII-25	−21	+41	16.36	1.22	+3.0	+1.3
BIII-35	−72	+21	16.06	0.83	+5.8	−7.2
BIII-41	−44	+6	15.80	1.33	−3.0	−1.0
(BIV-1)	+46	+74	15.01	1.28	−253.3	+1.3
BIV-9	+3	+51	15.76	0.84	−0.6	+2.9
BIV-17	+33	+48	16.09	0.97	+6.1	−0.3
BIV-31	+28	+28	16.50	1.00	+4.2	+7.6
BIV-49	+65	−1	16.46	1.19	−1.2	−4.0
BIV-63	+44	+10	16.13	1.07	+4.2	+3.0
CI-3	+129	−32	15.73	0.88	+7.6	−2.2
CI-8*	+99	−51	16.38	1.07	+18.4	−4.0
CI-24	+52	−90	16.61	1.09	+1.3	+0.1
CI-28	+53	−152	16.38	1.24	+1.3	+4.2
CI-29*	+3	−115	16.66	1.37	−38.3	−2.0
CII-6*	−25	−126	16.62	1.12	−10.9	+0.0
CII-9	−57	−101	16.37	1.25	+0.7	−2.7
(CII-20)	−85	−52	15.67	1.28	−148.2	+138.4
CII-23	−115	−42	16.36	1.14	−6.0	+0.0
CIII-3*	−106	−2	16.48	1.08	−13.8	+3.5
CIII-10	−154	+66	16.21	1.28	+0.0	+3.2
CIII-11	−114	+114	16.32	1.10	+2.0	+2.0
CIII-12	−66	+153	16.65	1.17	+2.9	−3.2
CIV-3*	+5	+138	16.57	1.01	−9.9	+1.3
CIV-12	+70	+64	16.53	1.28	+1.0	+7.1
CIV-19	+114	+60	16.51	1.20	+2.7	+3.0
CIV-24	+140	+4	15.70	0.82	+2.0	+0.0
CIV-26	+129	+23	16.89	1.03	−1.0	−0.1

TABLE 2

B. PROGRAM STARS FOR NGC 2164

Star (1)	x (arcsec) (2)	y (arcsec) (3)	V (4)	B−V (5)	v (km s⁻¹) (6)	δ (km s⁻¹) (7)
B15	+5	−21	15.60	1.17	+2.3	...
B18	+18	−19	15.39	1.25	+2.0	...
B25*	+20	−3	15.64	1.05	+6.3	−4.3
B34	+4	+1	15.40	1.15	+0.7	−1.6
C6	−5	+20	15.16	1.50	+4.3	...
C7*	+2	+28	15.41	1.40	−5.5	...
C8	+20	+41	15.64	1.22	+0.6	+0.6
C12	−36	+10	16.31	1.10	−1.4	...
C13	−27	+10	15.05	1.42	+0.3	...
C15	−27	−14	16.22	0.90	−1.2	...
C17	−18	−18	15.82	1.02	+2.3	...
D2*	+45	+56	15.68	1.24	+6.3	−3.2
(D7)	+2	+96	15.06	0.71	−235.3	+3.7
D12	−4	−61	15.92	1.13	−0.2	+5.3
(D14)	−14	−74	16.09	0.81	−276.3	−2.4
(H50)	+13	−52	16.53	0.92	−258.3	...

TABLE 2

C. PROGRAM STARS FOR NGC 2214

Star (1)	x (arcsec) (2)	y (arcsec) (3)	V (4)	$B-V$ (5)	v (km s^{-1}) (6)	δ (km s^{-1}) (7)
A100	+0	+2	14.48	1.37	−0.3	...
B18	−24	+9	14.92	0.47	−2.7	...
B54	+18	−13	15.76	1.33	+0.8	+0.4
B66	−24	−1	15.56	1.30	+0.4	+6.0
(C15)	−12	+53	15.55	1.32	−288.0	+1.0
C19*	−30	+36	15.31	0.73	+14.6	−1.2
C31	−40	−25	15.42	1.30	−2.0	+0.6
C40	−9	−40	15.61	1.39	+1.8	−1.4
(D1)	+43	+72	14.52	1.47	−280.0	...
D17	−59	+12	14.40	1.64	+1.8	...
(D39)	+58	−23	14.98	0.76	−244.2	...

NOTES.—Col. (1).—Identifications are from Robertson (1974) except for H50 in NGC 2164, which is from Flower and Hodge (1975). Names in parentheses are Galactic dwarfs or have discrepant measurements, and those with asterisks are probably LMC field stars. Cols. (2) and (3).—Distance from the center of the cluster in right ascension (x) and declination (y). Cols. (4) and (5).—Apparent V magnitude and $B-V$ color from Robertson (1974) except for H50 in NGC 2164, which is from Flower and Hodge (1975). Cols. (6) and (7).—Radial velocity $v \equiv \frac{1}{2}(v_{\rm I} + v_{\rm II})$ and velocity difference $\delta \equiv \frac{1}{2}(v_{\rm I} - v_{\rm II})$ from the two permutations of the fibers for NGC 1866 and NGC 2164 and from the two independent observations for NGC 2214. (The zeropoints are close to the mean velocities of the clusters.)

it was 0.3 km s^{-1}. Since these are small compared to the other errors discussed below, especially when added in quadrature, we can neglect uncertainties in the wavelength calibration.

The main sources of errors in the stellar velocities must therefore be photon noise, imperfect guiding, and the fiber/spectrograph system. Although we do not know exactly where the errors are introduced, their origin is not important provided that we include them correctly in our analysis. For this purpose, we use the velocity differences from the permutations of the fibers described above. Figure 2 shows the distribution of δ for NGC 1866 and a Gaussian with the same mean, 0.3 km s^{-1}, and standard deviation, $s_\delta = 3.3$ km s^{-1}. The distribution of δ for NGC 2164 is consistent with that for NGC 1866. Since the observational setup was identical for both clusters, we adopt for NGC 2164 the value of s_δ derived from the much larger NGC 1866 sample. The dispersion is $s_\delta = 2.7$ km s^{-1} for the six stars in NGC 2214 that have two independent measurements. Omitting B66, the star with the most discrepant value of δ, gives $s_\delta = 1.1$ km s^{-1}.

b) Contamination by Field Stars

The clusters in our sample were chosen in part because they lie in relatively uncrowded regions of the LMC. Nevertheless, some contamination by field stars is inevitable and this must be eliminated before we can estimate or set limits on the true velocity
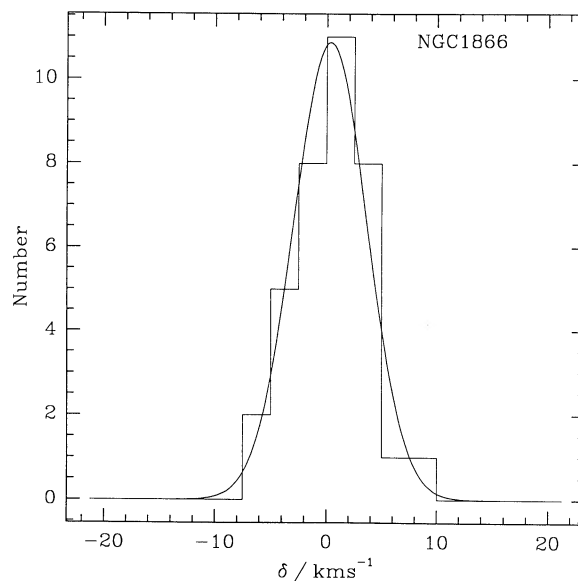
FIG. 2.—Histogram of the velocity differences δ for the program stars in NGC 1866. The smooth curve is a Gaussian distribution with a mean of 0.3 km s^{-1} and a standard deviation of 3.3 km s^{-1}.
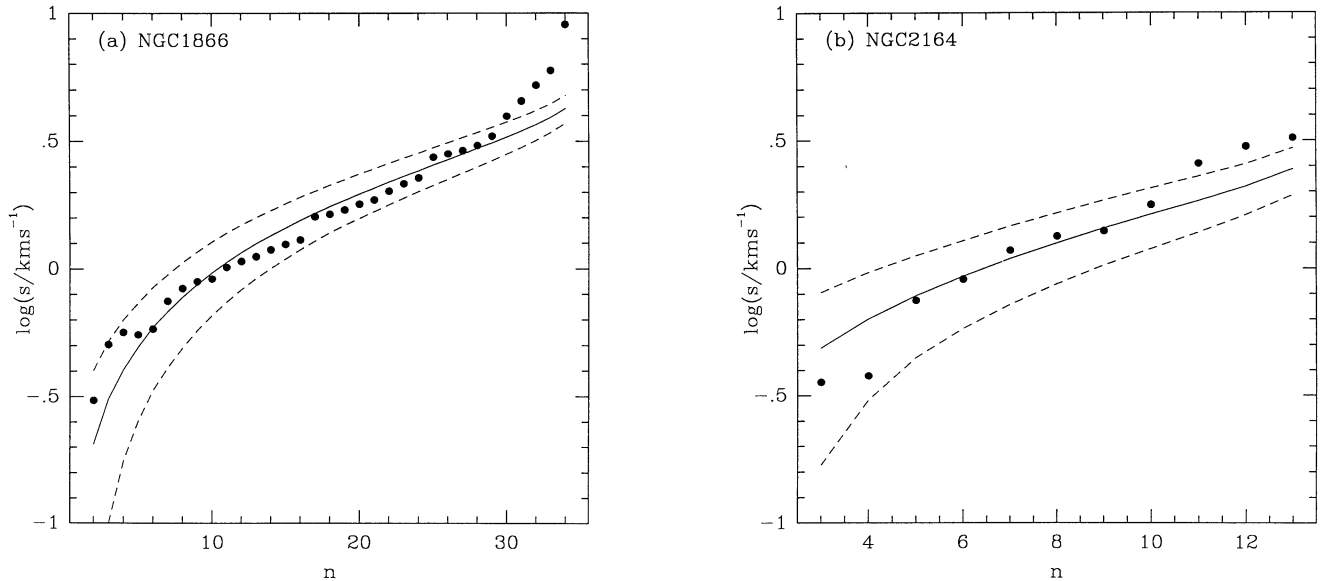
FIG. 3.—(*a–b*) Velocity dispersion $s_v(m, n)$ as a function of the number of stars remaining n when those with the highest velocities are removed for (*a*) NGC 1866 and (*b*) NGC 2164. The solid and dashed curves show the expected relations and one-sigma deviations from them for velocities drawn at random from Gaussian distributions.

dispersions of the clusters. We can safely assume that the stars with velocities differing from the means by more than 200 km s^{-1} are Galactic dwarfs, but we cannot arbitrarily reject the stars with less extreme velocities, such as CI-8 and CI-29 in NGC 1866 ($v = +18.4$ and -38.3 km s^{-1}, respectively). They could be field stars in the LMC or members of the cluster. We have therefore adopted the following scheme to make a reasonably objective choice of which stars to include.

Our first step is to compute the velocity dispersion using all m possible members of the cluster. We then remove the star with the velocity farthest from the mean and recompute the dispersion. The procedure is repeated to obtain $s_v(m, n)$, the velocity dispersion as a function of n, the number of stars remaining. We compare this with the corresponding relation for velocities drawn at random from a Gaussian distribution (as determined by a series of Monte Carlo simulations). If the sample is contaminated by field stars with a velocity dispersion higher than that of the cluster, the observed $s_v(m, n)$ will drop more rapidly with decreasing n than the Gaussian $s_v(m, n)$. However, this discrepancy will disappear at some value of n, and thereafter, the two relations will have nearly the same shape. The stars that must be rejected for the coincidence to occur are probably not members of the cluster.[1]

Figure 3*a* illustrates the above procedure for NGC 1866. After the removal of CII-20 and two Galactic dwarfs, there are $m = 34$ possible members. Since $s_v(m, n)$ agrees with the Gaussian relation for $n \lesssim 29$, the five stars with velocities farthest from the mean should be rejected. The remaining 29 stars have $s_v = 3.3$ km s^{-1}. As Figure 1*a* shows, the stars we have rejected (indicated by open and filled diamonds) are located in the outer parts of the cluster, where the probability of membership is lowest. From the star counts of EFF, we can estimate the surface density of stars brighter than $B \approx 17.5$ in the background. A comparison with the surface density of the cluster at the position of each of our program stars then gives the probability of its being a member. The sum of the probabilities for all the program stars is the expected number of members, and the balance is the expected number of Galactic and LMC field stars. On this basis, there should be about seven nonmembers, just the number we have rejected (when the Galactic dwarfs are included).

We now consider the contamination of our NGC 2164 and NGC 2214 samples. Three of the program stars in NGC 2164 are Galactic dwarfs, and the $m = 13$ possible members of the cluster have $s_v = 3.2$ km s^{-1}. A comparison of the observed and expected $s_v(m, n)$ relations, shown in Figure 3*b*, indicates that the three stars with the highest velocities should probably be rejected. The remaining 10 stars have $s_v = 1.8$ km s^{-1}. However, from the star counts, we expect only one or two nonmembers in our sample, and these have already been accounted for by the removal of the Galactic dwarfs. We therefore present the results derived with both 10 and 13 stars, which should encompass the full range of uncertainties. For NGC 2214, the choice of which stars to reject is much less ambiguous. Three of the program stars are Galactic dwarfs, and C19 has a velocity eight standard deviations from the others. Rejecting these four stars is consistent with the contamination we estimate from the star counts. We obtain $s_v = 1.8$ km s^{-1} for the remaining seven stars.

c) Velocity Dispersions

One might attempt to estimate the true velocity dispersions within the clusters from the simple formula $\sigma_v \approx (s_v^2 - s_\delta^2)^{1/2}$. However, this would be dangerous because s_v and s_δ are similar in magnitude, are affected by statistical uncertainties, and are not independent of each other. We must therefore adopt a more sophisticated approach. All the information we require is contained in

[1] The referee has drawn our attention to a method based on "probability plots" for estimating the contamination by field stars (see, for example, Lutz and Upgren 1980). This is essentially equivalent to our method, and it gives the same results.
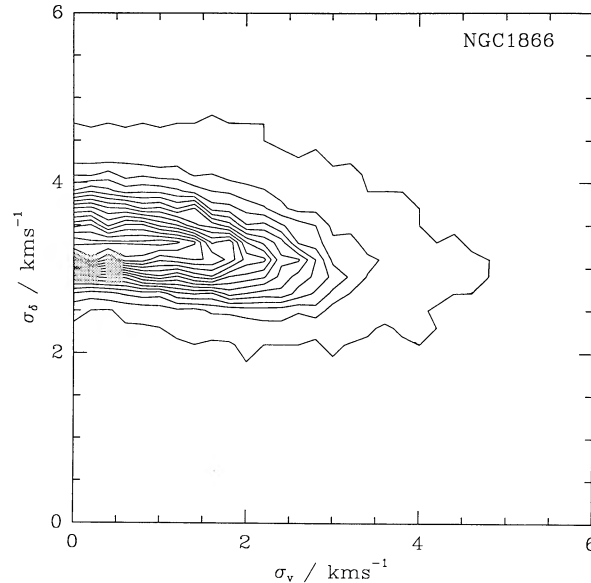
FIG. 4.—Contours of the probability density $p(\sigma_v, \sigma_\delta | s_v, s_\delta)$ in the $(\sigma_v, \sigma_\delta)$ plane for NGC 1866. The contours, at equal intervals of probability, were generated from the Monte Carlo simulations discussed in § IIIc.

the probability density $p(\sigma_v | s_v, s_\delta)$, i.e., the probability, given the observed dispersions s_v and s_δ, that the true velocity dispersion lies in a small interval near σ_v. Since s_v are σ_δ are not independent, it proves convenient first to compute the probability density $p(\sigma_v, \sigma_\delta | s_v, s_\delta)$, where σ_δ is the true (but unknown) dispersion in the errors.

We determine the probabilities from Monte Carlo simulations in which the velocities and errors are drawn at random from Gaussian distributions with standard deviations σ_v and σ_δ. At each point on a grid of $(\sigma_v, \sigma_\delta)$, we generate many samples of n stars, where $n = 29, 13$ (or 10), and 7, respectively, for NGC 1866, NGC 2164, and NGC 2214. We then compute the dispersions s_v and s_δ in the same way as for the real data, taking into account the number of independent measurements of the velocity of each star. Since the samples are relatively small, the "output" dispersions (s_v, s_δ) generally differ from the "input" dispersions $(\sigma_v, \sigma_\delta)$. The probability density $p(\sigma_v, \sigma_\delta | s_v, s_\delta)$ is proportional to the number of simulations in which s_v and s_δ lie within small intervals near the observed values. We repeat the procedure for each point on the grid, and thus generate probability contours in the $(\sigma_v, \sigma_\delta)$ plane. These are shown for NGC 1866 in Figure 4.

We obtain $p(\sigma_v | s_v, s_\delta)$ simply by integrating $p(\sigma_v, \sigma_\delta | s_v, s_\delta)$ over all values of σ_δ. The results are shown in Figures 5a–5c along with the corresponding cumulative probabilities $P(<\sigma_v | s_v, s_\delta)$. Since there are no obvious peaks in $p(\sigma_v | s_v, s_\delta)$ at nonzero values of σ_v, we cannot determine the actual velocity dispersions within the clusters. We can, however, assign upper limits from the cumulative probabilities. At the 95% confidence level, these are 2.9 km s^{-1} for NGC 1866 and 4.3 km s^{-1} (13 stars) or 2.9 km s^{-1} (10 stars) for NGC 2164. We have two values of s_δ for NGC 2214, depending on whether the contribution from the star B66 is included. However, this hardly affects the 95% confidence limits on σ_v, which are 3.9 and 3.5 km s^{-1} in the two cases. We adopt the more conservative limit. The values of s_v and s_δ and the limits on σ_v for the three clusters in our sample are summarized in Table 3.

It is worth noting at this stage that the velocity dispersions s_v and σ_v might include contributions from the relative motions of binary stars. However, only the contributions from their center-of-mass motions should be used when estimating the masses of the clusters. Any corrections for binaries would be highly uncertain but could only strengthen the limits derived in this paper. Another

TABLE 3

VELOCITY DISPERSIONS AND RELATED QUANTITIES

Quantity	NGC 1866	NGC 2164		NGC 2214
$s_v/\text{km s}^{-1}$	3.3	3.2	1.8	1.8
$s_\delta/\text{km s}^{-1}$	3.3	(3.3)	(3.3)	2.7
$\sigma_v/\text{km s}^{-1}$	<2.9	<4.3	<2.9	<3.9
$\langle I \rangle_{\text{iso}}$	0.47	0.47	0.49	0.74
$\langle I \rangle_{\text{rad}}$	0.21	0.30	0.34	0.57

NOTES.—The quantities s_v and s_δ are the standard deviations of the radial velocities $v \equiv \frac{1}{2}(v_\text{I} + v_\text{II})$ and the velocity differences $\delta \equiv \frac{1}{2}(v_\text{I} - v_\text{II})$. The 95% confidence limits on σ_v are from the Monte Carlo simulations discussed in § IIIc. The values of $\langle I \rangle_{\text{iso}}$ and $\langle I \rangle_{\text{rad}}$ are weighted means of eq. (10) over the positions of the program stars for the extreme cases of isotropic and purely radial velocity distributions. For NGC 2164, the values in the first column are based on 13 stars, and those in the second column are based on 10 stars.
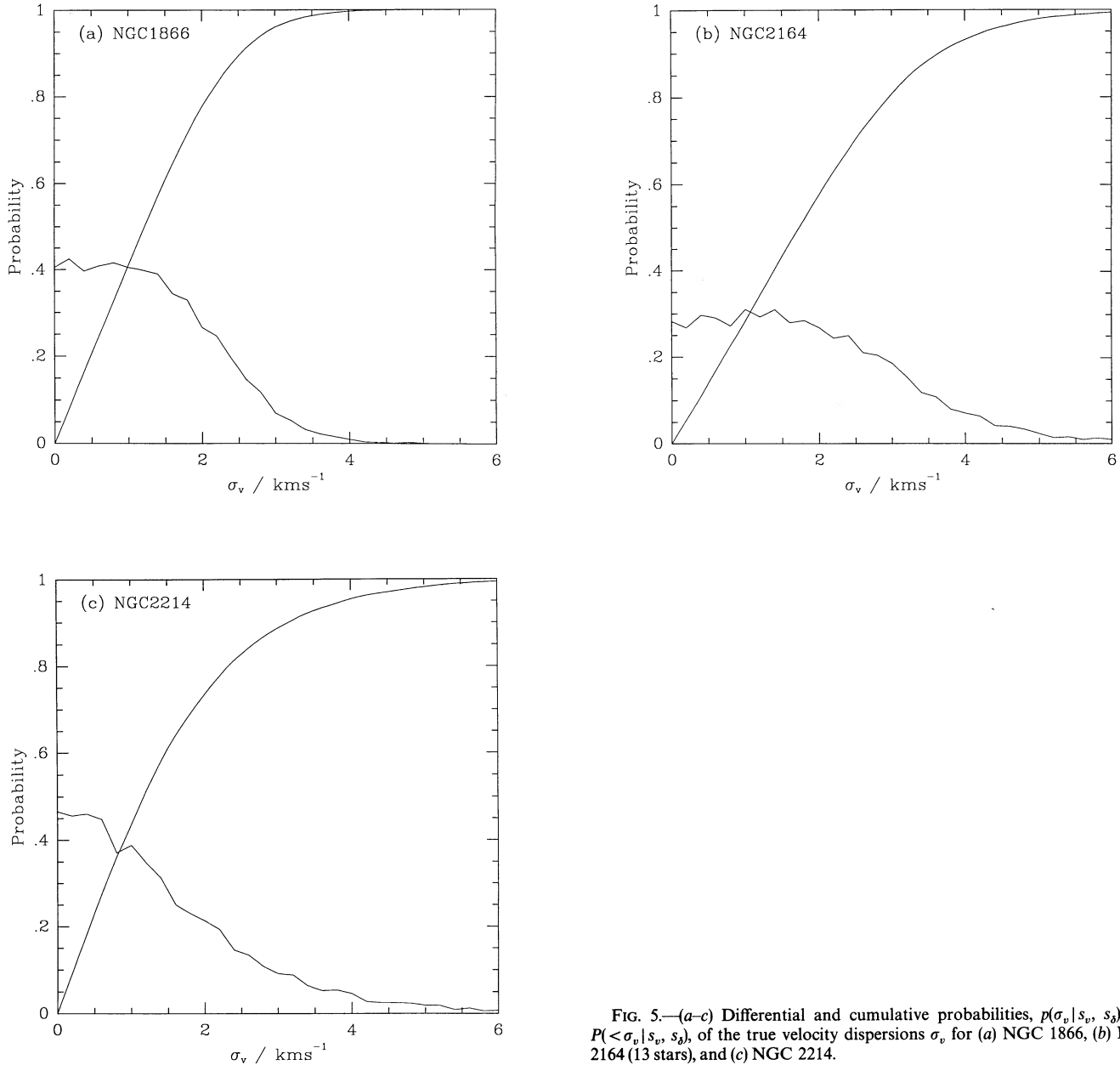
FIG. 5.—(a–c) Differential and cumulative probabilities, $p(\sigma_v | s_v, s_\delta)$ and $P(<\sigma_v | s_v, s_\delta)$, of the true velocity dispersions σ_v for (a) NGC 1866, (b) NGC 2164 (13 stars), and (c) NGC 2214.

concern is that s_v and σ_v could be affected by any rotation of the clusters. There is no evidence for rotation in our data, but given the relatively large errors, this is only a weak constraint. Some indication that rotation is not dynamically important comes from the shapes of the clusters. The apparent ellipticities, measured near the median radii r_h, are $\epsilon = 0.08 \pm 0.06$ for NGC 1866, $\epsilon = 0.13 \pm 0.08$ for NGC 2164, and $\epsilon = 0.28 \pm 0.08$ for NGC 2214 (Frenk and Fall 1982). Using equations (52)–(54) of Fall and Frenk (1983), we estimate that the ratios of rotational to random kinetic energy $T_{\rm rot}/T_{\rm rand}$ are of order 10%, with the exact values depending on the unknown inclination angles and velocity anisotropies of the clusters.

IV. TOTAL MASSES AND RELATED QUANTITIES

We now use the results of the previous section to set limits on the central densities, total masses, and mass-to-light ratios of the clusters. The projected velocity dispersion $\sigma_p(R)$ at a projected radius R from the center of a spherical, nonrotating cluster is related to the volume density $\rho(r)$ at an unprojected radius r and the velocity dispersions $\sigma_r(r)$ and $\sigma_t(r)$ in the radial and tangential directions by

$$\sigma_p^2(R) = \frac{2}{\mu(R)} \int_R^\infty dr \, \frac{\rho(r)[(r^2 - R^2)\sigma_r^2(r) + R^2\sigma_t^2(r)]}{r(r^2 - R^2)^{1/2}} , \tag{2}$$

(Binney and Tremaine 1987, p. 208). We assume that the mass-to-light ratio is constant throughout each cluster and therefore that $\mu(R)$ and $\rho(r)$ can be interpreted in the following discussion as the projected and unprojected mass densities. The functions $\rho(r)$, $\sigma_r(r)$, and $\sigma_t(r)$ must satisfy the equations of stellar hydrodynamics; for a spherical, nonrotating cluster in a steady state, these reduce to

$$\frac{1}{\rho}\frac{d}{dr}(\rho\sigma_r^2) + \frac{2}{r}(\sigma_r^2 - \sigma_t^2) = -\frac{GM(r)}{r^2} , \tag{3}$$

where

$$M(r) = 4\pi \int_0^r dr' r'^2 \rho(r') \tag{4}$$

is the mass contained within a sphere of radius r.

To make further progress, we consider models in which the radial and tangential velocity dispersions are related by

$$\sigma_t^2(r) = \sigma_r^2(r)/[1 + (r/r_a)^2] , \tag{5}$$

with the "anisotropy radius" r_a left as a free parameter. For $r \lesssim r_a$, the stellar orbits are nearly isotropic, whereas at larger radii, they are predominantly radial. The solution of equation (3), with the assumed relation between σ_r and σ_t, is then

$$\rho(r)\sigma_r^2(r) = \frac{G}{(r^2 + r_a^2)} \int_r^\infty dr' \left[1 + \left(\frac{r_a}{r'}\right)^2\right]\rho(r')M(r') , \tag{6}$$

(Binney 1980). Equations (5) and (6) are consequences of any distribution function that depends on the energy E and angular momentum J through the combination $Q \equiv E + \frac{1}{2}(J/r_a)^2$. The distribution function $f(Q)$ is uniquely determined by $\rho(r)$ but seldom is the relation simple (Osipkov 1979; Merritt 1985).

The deprojected density profile corresponding to equation (1) is

$$\rho(r) = \rho_0[1 + (r/a)^2]^{-(\gamma+1)/2} , \tag{7}$$

where

$$\rho_0 = \frac{\mu_0 \Gamma(\gamma/2 + \frac{1}{2})}{\sqrt{\pi}\, a\Gamma(\gamma/2)} \tag{8}$$

is the central density and Γ denotes the usual gamma function. In this case, equations (1), (2), and (5)–(8) give

$$\sigma_p^2(R) = \rho_0 a^2 G I(R/a;\, r_a/a,\, \gamma) ; \tag{9}$$

the nondimensional function above is defined by

$$I(x;\, \alpha,\, \gamma) \equiv \frac{4\sqrt{\pi}\,\Gamma(\gamma/2 + 1/2)(1 + x^2)^{\gamma/2}}{\Gamma(\gamma/2)(\alpha^2 + x^2)^{1/2}} \int_x^\infty dy(1 + y^2)^{-(\gamma+1)/2}\left(1 + \frac{\alpha^2}{y^2}\right)J(y;\, \gamma)$$

$$\times \left[\left(\frac{2\alpha^2 + x^2}{\alpha^2 + x^2}\right)\text{Arctan}\left(\frac{y^2 - x^2}{\alpha^2 + x^2}\right)^{1/2} - \left(\frac{y^2 - x^2}{\alpha^2 + x^2}\right)^{1/2}\left(\frac{x^2}{y^2 + \alpha^2}\right)\right], \tag{10a}$$

and

$$J(y;\, \gamma) \equiv \int_0^y dz\, z^2(1 + z^2)^{-(\gamma+1)/2} \tag{10b}$$

is an incomplete beta function. Figure 6 shows the dependence of I on R/a for several values of r_a/a and $\gamma = 2.55$, the index appropriate for NGC 1866. Evidently, the projected velocity dispersion is several times smaller at the positions of the program stars than it is at the center of the cluster.

For comparison with our empirical limits on the velocity dispersions, we average equation (9) over the positions of the program stars and set $\sigma_v^2 = \langle\sigma_p^2(R)\rangle$. Our estimate of the central density is then

$$\rho_0 = \frac{\sigma_v^2}{a^2 G\langle I\rangle} . \tag{11}$$

The analogous estimate of the total mass, from equations (4), (7), (8), and (11), is

$$M_\infty = \frac{2\pi^{3/2}\Gamma(\gamma/2)a\sigma_v^2}{(\gamma - 2)\Gamma(\gamma/2 + 1/2)G\langle I\rangle} . \tag{12}$$

In these expressions, $\langle I\rangle$ denotes $\sum w_i I(R_i/a;\, r_a/a,\, \gamma)/\sum w_i$, where the sums are over all the program stars and weights w_i are the number of independent measurements of the velocities. We consider the two extremes $r_a/a = \infty$ and $r_a/a = 0$, corresponding to isotropic and purely radial velocity distributions. The values of $\langle I\rangle$ for both cases are listed in Table 3. In principle, we could ignore small values of r_a/a on the grounds that the clusters would be unstable to nonradial perturbations and would become highly flattened on their dynamical time scales if the orbits were too radial. The models studied by Merritt and Aguilar (1985), with velocity

LUPTON *ET AL.*
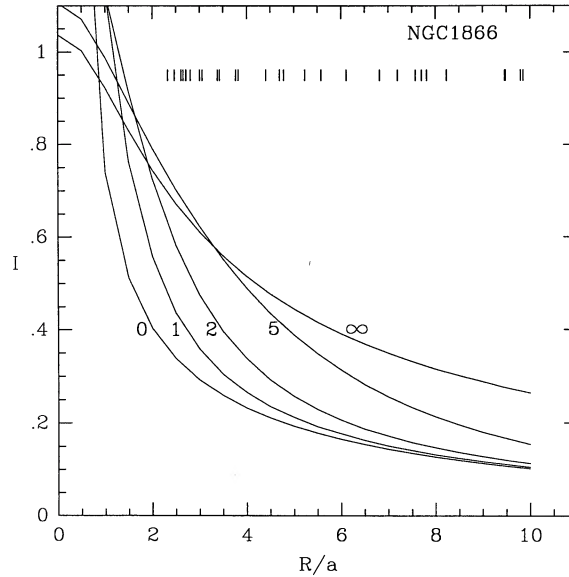
FIG. 6.—Radial dependence of the nondimensional function I defined by eq. (10) for $\gamma = 2.55$ and five values of the anisotropy radius. The curves are labeled by the values of r_a/a. The short vertical marks indicate the positions of the program stars in NGC 1866.

dispersions satisfying equation (5), are unstable for $r_a/r_h \lesssim 0.3$. However, since $\langle I \rangle$ changes only slowly over this range, we do not in practice obtain useful constraints on ρ_0 and M_∞ from such arguments.

In the derivation of equations (11) and (12), we have neglected the tidal field of the LMC and any mass segregation within the clusters. All our program stars are closer to the centers of the cluster than one-third the tidal radii calculated in the next section. At these positions, the addition of a tidal term in the equations of stellar hydrodynamics would change the solutions by less than a few percent (see Fig. 14 of EFF). Thus, equation (12) gives very nearly the correct total mass, even if the cluster has an unbound halo, provided there is no mass segregation, and hence that the mass-to-light ratio does not vary with radius. EFF fitted equation (1) separately to the star counts on plates of the same cluster with different limiting magnitudes, corresponding to a range in stellar masses from 1.5 to about 5 $M_\odot$. No mass segregation was found in NGC 2164 or NGC 2214. There is marginally significant evidence that the brightest stars in NGC 1866 are more centrally concentrated than the faintest stars; but the effect is small ($\Delta\gamma \approx 0.5$) and only introduces uncertainties of order 10% in ρ_0 and M_∞.

The central densities and total masses of the clusters derived from the 95% confidence limits on σ_v are listed in Table 4. We give the results separately for isotropic and purely radial velocity distributions; the limits are 20% to 50% smaller for $r_a/a = \infty$ than they are for $r_a/a = 0$. For the three clusters in our sample, the limits on ρ_0 range from 200 to 2400 $M_\odot$ pc^{-3}, and the limits on M_∞ range from 1.2 to 8 × 10^5 $M_\odot$. We have divided the limits on M_∞ by the asymptotic (integrated) luminosities $L_{V\infty}$ from EFF to set upper limits on the global mass-to-light ratios of the clusters. These range from 0.4 to 1.4 in solar units and are also listed in Table 4. Possible errors in the core parameters a introduce uncertainties of up to 50% in ρ_0, but they have little effect on either M_∞ or $M_\infty/L_{V\infty}$ (because most of the velocities were measured outside the cores). Since a is directly proportional to the distance D to the LMC, we obtain from equations (11) and (12) the following scalings: $\rho_0 \propto D^{-2}$, $M_\infty \propto D$, and $M_\infty/L_{V\infty} \propto D^{-1}$. Thus, with a distance of 50 kpc instead of the value 55 kpc assumed here, the limits on $M_\infty/L_{V\infty}$ would increase by 10%.

In principle, our limits on the mass-to-light ratios can be used to place constraints on the stellar content of the clusters. EFF and Elson, Fall, and Freeman (1989) estimated the mass-to-light ratios from stellar population models with IMFs of the form: $\phi(m) \propto m^{-1-x}$ for $m_l \leq m \leq m_u$ and $\phi(m) = 0$ for $m < m_l$ and $m > m_u$. The lower cutoff m_l was allowed to vary from 0.1 to 0.5 $M_\odot$ and the upper cutoff m_u from 35 to 100 $M_\odot$. (Both cutoffs involve large extrapolation because the observable range of stellar masses is only $1.5 \lesssim m \lesssim 5$ $M_\odot$.) In the first study, a wide range of IMF slopes was considered ($1.1 \leq x \leq 2.2$), whereas in the second study, the observed values ($-0.2 \leq x \leq 0.8$) were used. All the models with flat IMFs are consistent with our upper limits on the mass-to-light ratios. The models with $x = 2.2$ and $m_l = 0.5$ $M_\odot$ are also acceptable, but the models with $x = 2.2$ and $m_l = 0.1$ $M_\odot$ are marginally ruled out. More useful constraints on the stellar content of the clusters will probably require actual measurements of the velocity dispersions.

V. TIDAL RADII AND UNBOUND HALOS

We now consider the suggestion by EFF that the young clusters in the LMC have unbound halos. Since the motions of the young clusters are similar to those of other Population I objects in the LMC, their orbits must be nearly circular (Freeman, Illingworth, and Oemler 1983). According to King (1962), the tidal radius of a cluster with a mass M_t on a circular orbit is given by

$$r_t = \left(\frac{GM_t}{4\Omega^2 - \kappa^2} \right)^{1/3} , \tag{13}$$

TABLE 4

UPPER LIMITS ON THE CENTRAL DENSITIES, TOTAL MASSES, MASS-TO-LIGHT RATIOS, AND TIDAL RADII

QUANTITY	NGC 1866		NGC 2164				NGC 2214	
$\log (\rho_0/M_\odot \text{ pc}^{-3})$	2.31	2.66	3.20	3.39	2.84	3.00	2.75	2.86
$\log (M_\infty/M_\odot)$	5.57	5.92	5.45	5.64	5.09	5.25	5.59	5.71
$\log (M_\infty/L_{V\infty})$	−0.44	−0.09	−0.07	0.12	−0.43	−0.27	0.04	0.16
$\log (r_t/\text{arcsec})$	2.60	2.74	2.68	2.77	2.53	2.60	2.73	2.78

NOTES.—All entries are based on the 95% confidence limits on σ_v from Table 3. The first column for each cluster refers to isotropic and the second to purely radial velocity distributions. For NGC 2164, the limits in the first pair of columns are based on 13 stars, and those in the second pair of columns are based on 10 stars.

where Ω and κ are, respectively, the circular and epicyclic frequencies of the parent galaxy at the position of the cluster. We use the estimates of the tidal field of the LMC given by EFF. For the three clusters in our sample, which are located far from the center of the LMC, the values of $4\Omega^2 - \kappa^2$ are probably accurate to better than ±30%. This is adequate for our purpose because the tidal field enters equation (13) only to the one-third power.

King's formula merely gives the distance between the center of an object and its inner or outer Lagrangian points. It should therefore be considered as an approximation to the tidal radius of a real cluster. In particular, equation (13) neglects the compression of the Roche surface in the direction orthogonal to the center of the parent galaxy. Moreover, some families of orbits that are not formally bound to a cluster have remarkably stable behavior over long intervals of time. The validity of King's formula has been tested by numerical integrations of the restricted three-body problem, but unfortunately, the results are not conclusive. Keenan (1981a, b) finds that the effective tidal radius of a cluster is only two-thirds of that given by equation (13), whereas Seitzer (1983, 1985) finds that the coefficient is close to unity. We adopt King's formula for the tidal radius because it almost certainly leads to conservative estimates of the masses of any unbound halos.

It is instructive to compare the observed profiles of the clusters in our sample with King (1966) models that have central densities ρ_0 equal to the upper limits derived in the previous section, core radii r_c equal to the observed values, and tidal radii r_t fixed by equation (13). The last constraint deserves special emphasis because, in most studies of Galactic globular clusters, the parameter r_t is determined by fitting models to the observed profiles without any reference to a tidal field. Our procedure is the same as the one adopted by EFF, except that here ρ_0 is fixed by the empirical limits on the velocity dispersions rather than the mass-to-light ratios from stellar population models. The mass of a King model can be expressed as

$$M_t = \rho_0 r_c^3 g(c) , \qquad (14)$$

where $c \equiv \log (r_t/r_c)$ is the concentration parameter and $g(c)$ is a known function. We solve for c and hence r_t using equations (13) and (14). Since both $4\Omega^2 - \kappa^2$ and ρ_0 scale with the distance to the LMC as D^{-2}, we have $r_t \propto D$.

The tidal radii derived from the 95% confidence limits on σ_v, with both isotropic and purely radial velocity distributions, are listed in Table 4. As the anisotropy radii r_a decrease from ∞ to 0, the values of r_t increase by 10% to 40%. Our limits are in the middle of the ranges computed by EFF for NGC 1866 and NGC 2164 and at the upper end of the range for NGC 2214. They are nearly identical to the limits that would be obtained simply by truncating the deprojected profiles, in the form of equation (7), at values of r_t satisfying equation (13). We have also checked that Michie models, the anisotropic analogs of King models, give very similar results. Since most of the mass is in the outer parts of the clusters, the limits on r_t are hardly affected by errors or evolution in the core parameters ρ_0 and r_c. Thus, it seems reasonable to interpret the entries in Table 4 as upper limits on the "eventual" tidal radii. Even if this interpretation turns out not to be correct, the limits on r_t should provide some indication of whether or not the clusters currently have unbound halos.

Figures 7a–7c show for each cluster in our sample the observed surface brightness profile from EFF. These are plotted out to the maximum radii $r_{\max}$ at which the clusters could be distinguished from the backgrounds. Also shown are the projected profiles of the King models derived by the above procedure and normalized to agree with the observed central surface brightnesses. The outer solid curves correspond to the 95% confidence limits on σ_v, while the inner solid curves correspond to the 50% confidence limits, assuming in both cases that the velocity distributions are isotropic. For NGC 2164, we have plotted the results based on 13 stars, which are more conservative than those based on 10 stars. The relation $r_t \propto D$ implies that Figures 7a–7c are not affected by uncertainties in the distance to the LMC. In particular, the ratio $r_t/r_{\max}$ is invariant.

The observed profile of NGC 1866 extends well beyond the King model with our 95% confidence limit on the tidal radius for an isotropic velocity distribution. In this case, the mass bound to the cluster M_t is less than $2.5 \times 10^5 M_\odot$, leaving more than 30% of the total mass in an unbound halo. The 95% confidence limit on r_t is slightly larger than $r_{\max}$ for a purely radial velocity distribution. However, even in this extreme case, any model with reasonably smooth behavior near the tidal radius (such as a Michie model) would fall below the observed profile. For the other clusters in our sample, NGC 2164 and NGC 2214, the situation is less clear. The observed profiles extend beyond the King models with the 50% confidence limits on r_t but not those with the 95% confidence limits. Thus, we cannot be certain that the clusters have unbound halos. If the formula for the tidal radius preferred by Keenan (1981a, b) were adopted, the evidence for an unbound halo around NGC 2164 would be marginal while that for an unbound halo around NGC 2214 would be compelling. We conclude that at least one and possibly all three clusters in our sample are not yet tidally limited by the LMC.
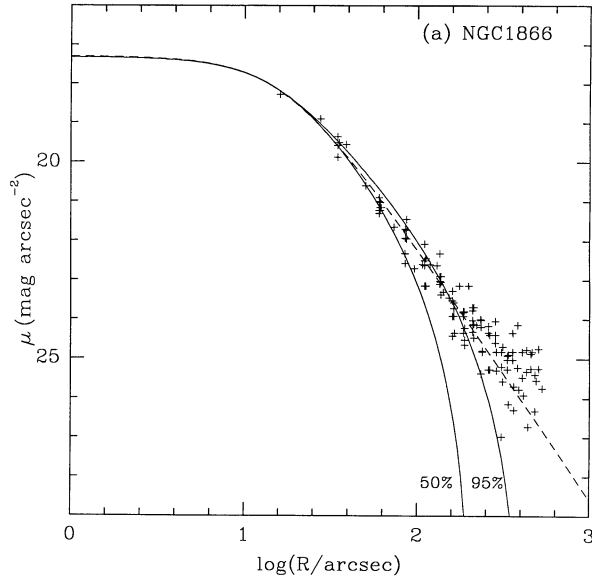
FIG. 7*a*
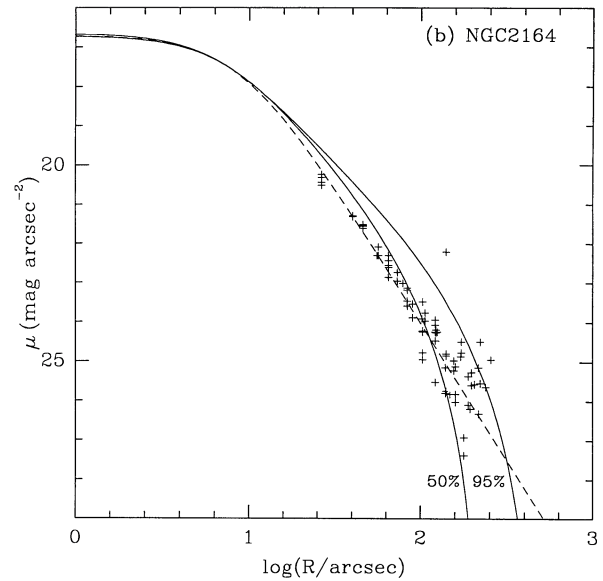
FIG. 7*b*
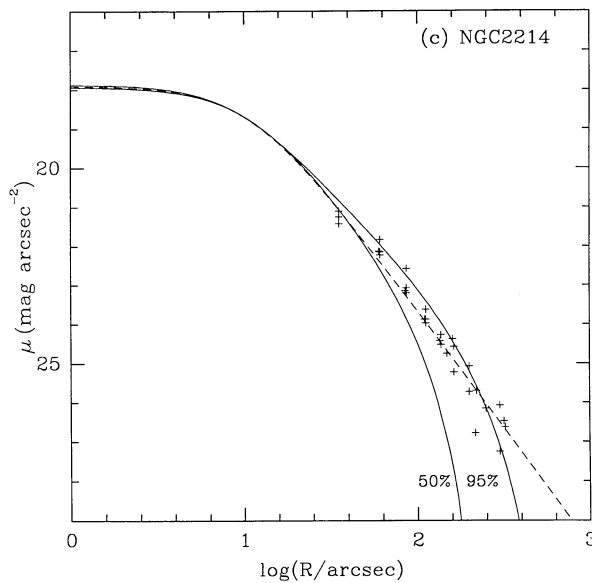
FIG. 7*c*

FIG. 7.—(*a–c*) Surface brightness profiles from the star counts of Elson, Fall, and Freeman (1987) for (*a*) NGC 1866, (*b*) NGC 2164, and (*c*) NGC 2214. The dashed curves are given by eq. (1) with the parameters listed in Table 1. The solid curves are King (1966) models with tidal radii computed from the 95% and 50% confidence limits on σ_v by the method described in § V.

Are the unbound halos surprising? One might suppose that the gas clouds from which the clusters formed were tidally limited by the LMC. If so, any subsequent mass loss would cause the protoclusters to expand, and their outer parts would become unbound. The gas that was not used up in the formation of stars would almost certainly be expelled by some combination of stellar winds and supernovae. Moreover, even after all the residual gas had been removed, clusters with flat IMFs could still lose a significant fraction of their masses in the form of stellar ejecta. These possibilities are discussed in more detail by Elson, Fall, and Freeman (1989). Since the clusters in our sample are located 3.7 to 5.2 kpc from the center of the LMC, where the rotation periods are 3 to 5 × 10^8 yr, they have completed only small fractions of their orbits. The numerical simulations by Keenan (1981*a, b*) and Seitzer (1983, 1985) indicate that the unbound halo of a cluster will survive for 5 to 10 orbits around the parent galaxy. At that time, the clusters in our sample might resemble the tidally limited King models plotted in Figures 7*a*–7*c*. Finally, we note that the Hyades, the only Galactic cluster for which a complete census of the members has been made from proper motions, also appears to have an unbound halo (Pels, Oort, and Pels-Kluyver 1975).

REFERENCES

Binney, J. 1980, *M.N.R.A.S.*, **190**, 873.
Binney, J., and Tremaine, S. 1987, *Galactic Astronomy* (Princeton: Princeton University Press).
Elson, R. A. W., Fall, S. M., and Freeman, K. C. 1987, *Ap. J.*, **323**, 54 (EFF).
———. 1989, *Ap. J.*, **336**, 734.
Elson, R. A. W., and Freeman, K. C. 1985, *Ap. J.*, **288**, 521.
Fall, S. M., and Frenk, C. S. 1983, *A.J.*, **88**, 1626.
Flower, P. J., and Hodge, P. W. 1975, *Ap. J.*, **196**, 369.
Freeman, K. C., Illingworth, G., and Oemler, A. 1983, *Ap. J.*, **272**, 488.
Frenk, C. S., and Fall, S. M. 1982, *M.N.R.A.S.*, **199**, 565.
Illingworth, G. 1976, *Ap. J.*, **204**, 73.
Keenan, D. W. 1981a, *Astr. Ap.*, **95**, 334.
———. 1981b, *Astr. Ap.*, **95**, 340.

King, I. 1962, *A.J.*, **67**, 471.
———. 1966, *A.J.*, **71**, 64.
Lupton, R. H., Gunn, J. E., and Griffin, R. F. 1987, *A.J.*, **93**, 1114.
Lutz, T. E., and Upgren, A. R. 1980, *A.J.*, **85**, 1390.
Merritt, D. 1985, *A.J.*, **90**, 1027.
Merritt, D., and Aguilar, L. A. 1985, *M.N.R.A.S.*, **217**, 787.
Osipkov, L. P. 1979, *Astr. Zh. Pis'ma*, **5**, 77.
Pels, G., Oort, J. H., and Pels-Kluyver, H. A. 1975, *Astr. Ap.*, **43**, 423.
Robertson, J. W. 1974, *Astr. Ap. Suppl.*, **15**, 261.
Seitzer, P. 1983, Ph.D. thesis, University of Virginia.
———. 1985, in *IAU Symposium 113, Dynamics of Star Clusters*, ed. J. Goodman and P. Hut (Dordrecht: Reidel), p. 343.

Rebecca A. W. Elson: Institute for Advanced Study, Olden Lane, Princeton, NJ   08540

S. Michael Fall: Space Telescope Science Institute, 3700 San Martin Drive, Baltimore, MD   21218

Kenneth C. Freeman: Mount Stromlo and Siding Spring Observatories, Private Bag, Woden PO, ACT 2606, Australia

Robert H. Lupton: Institute for Astronomy, 2680 Woodlawn Drive, Honolulu, HI   96822